Advances in Science and Technology Research Journal

Advances in Science and Technology Research Journal 2024, 18(1), 291–305
https://doi.org/10.12913/22998624/178463
ISSN 2299-8624, License CC-BY 4.0

Received: 2023.09.28
Accepted: 2024.01.04
Published: 2024.01.16

The Effect of Re Content on Microstructure and Creep Resistance of Single Crystal Castings Made of Nickel-Based Superalloys

Kamil Gancarczyk[1*], Robert Albrecht[2], Małgorzata Kawalec[3], Barbara Kościelniak[1], Andrzej Gradzik[1], Dariusz Szeliga[1], Andrzej Kawalec[4], Waldemar Ziaja[1], Maciej Motyka[1]

[1] Department of Materials Science and Research and Development Laboratory for Aerospace Materials, Faculty of Mechanical Engineering and Aeronautics, Rzeszow University of Technology, 12 Powstancow Warszawy Ave., 35-959 Rzeszow, Poland

[2] Institute of Materials Science, University of Silesia, 1a 75 Pulku Piechoty Str., 41-500 Chorzow, Poland

[3] Department of Manufacturing Processes and Production Engineering, Faculty of Mechanical Engineering and Aeronautics, Rzeszow University of Technology, 12 Powstancow Warszawy Ave., 35-959 Rzeszow, Poland

[4] Department of Manufacturing Techniques and Automation, Faculty of Mechanical Engineering and Aeronautics, Rzeszow University of Technology, 12 Powstancow Warszawy Ave., 35-959 Rzeszow, Poland

* Corresponding author's e-mail: kamilgancarczyk@prz.edu.pl

ABSTRACT

In this work the effect of crystal structure perfection on the creep resistance of single crystal superalloys. The CMSX-4 and CMSX-4®Plus with increased Re content is analyzed. Single crystal rods are made by directional solidification process at the withdrawal rates 3 and 5 mm/min. The evaluation of microstructure and crystal structure perfection are carried out by light microscopy and X-ray diffraction Ω-scan methods. Creep tests are performed according to ASTM E-139-11 standard at the temperature of 982 °C. Mathematical models for the creep resistance of the models are developed for both investigated superalloys. The influence of the crystal structure on the the investigated superalloys are built and the steady state creep rates are determined. Creep strength of both superalloys are compared. The results show that the CMSX-4®Plus nickel superalloy exhibits nearly two times higher creep resistance compared to the conventional CMSX-4 one.

Keywords: mathematical models, creep resistance, CMSX-4®Plus, crystal structure perfection, CMSX-4, statistical analysis, nickel alloy, superalloy.

INTRODUCTION

The continuous improvement of aircraft engines efficiency depends highly on the development and application of new heat-resistant materials for the critical components of high pressure turbine. Currently single crystal (SX) nickel-based superalloys castings are used for the manufacturing of hot sections elements, such as blades and vanes. The Bridgman-Stockbarger method is most often used process in production of SX components. Application of the starter block and grain selector in the ceramic mold, and proper selection of the solidification process conditions enables production of castings without grain boundaries. Hence, such materials can be treated very roughly as imprefect single crystals. The SX castings exhibit much higher creep resistance and are able to operate at higher temperature – up to 1150 °C, compared to conventional polycrystalline nickel-based superalloys [1-5].

The crystal structure of single crystals nickel-based superalloys has a significant influence on their mechanical properties at high temperature. The essential parameter of Bridgman-Stockbarger SX casting process is withdrawal rate of the ceramic mold. Selection of proper withdrawal rate enables manufacturing of castings featuring

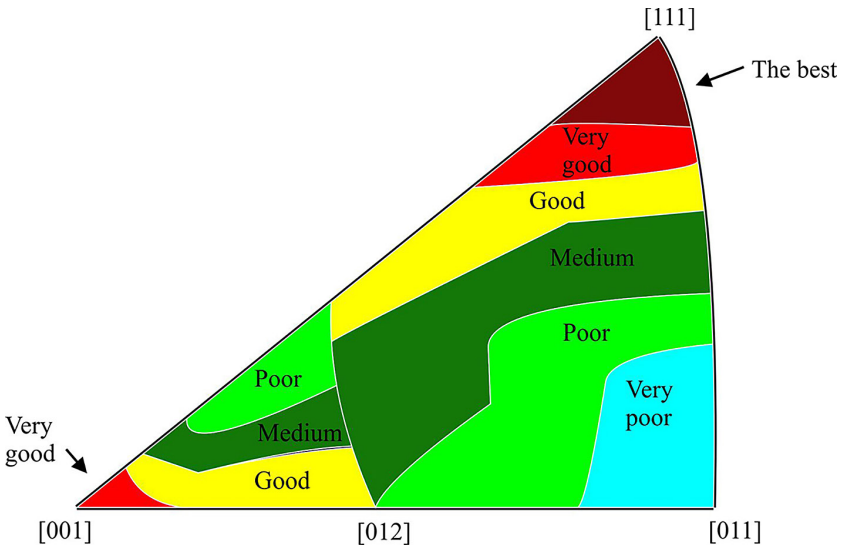

Fig. 1. The influence of the crystal orientation of MAR247 nickel superalloy on their creep strange [1]

high perfection of the crystal structure. The elemental parameter used to define the degree of crystal structure perfection is the value of the deviation angle α_z between the crystallographic direction [001] and the withdrawal direction of the blade. The high value of α_z (>15°) can significantly reduce the creep resistance of SX turbine blades [6-11] (Fig. 1).

The crystal structure perfection and creep strength of single crystal castings can be improved by modification of superalloys chemical composition. A number of multicomponent nickel-based superalloys have been developed to allow obtaining single crystal structure during the casting process. Presently, SX nickel superalloys are manufactured mainly by Cannon Muskegon and General Electric [12-17].

Due to the complex chemical composition of superalloys, single crystal nickel-based superalloys are classified in six generations [12, 13]. The chemical composition of single-crystal superalloys of the 1st generation, compared to conventional, directionally crystallized alloys, is characterized by the lack of elements segregating to grain boundaries – C, B and Zr [14]. In the 2nd generation superalloys, the addition of Re (approx. 3%) was introduced [16]. 3rd generation superalloys are characterized by a higher Re content (up to 5÷6%) and a lower Cr content [18]. The fourth generation of single-crystalline nickel superalloys is characterized by a Ru content compared to the previous ones. The development of the 5th and 6th generation of nickel superalloys is aimed at increasing their operating temperature and reducing defects in their structure [19]. Alloying elements of superalloy can be classified in terms of their influence on the microstructure and properties, i.e. on:

- forming strengthening of solid solution (γ phase matrix) – Ni, Co, Cr, Mo, Re, Ru and W,
- forming precipitations of the strengthening phase γ‘ – Al, Ta and Ti.

Currently the second-generation CMSX-4 superalloy is most often used for production of high pressure turbine blades in aircraft engines. The CMSX-4 alloy is distinguished by significant concentration of Re (approx. 3%) which increases the dispersion of the γ′ phase precipitates, reduces the mismatch between lattice constants value of the γ and γ′ phase ($a_{0\gamma}$ and $a_{0\gamma'}$) and promotes the γ phase solution strengthening effect. Recently, a new CMSX-4®Plus superalloy has been developed as a prospective one. The CMSX-4®Plus alloy has increased concentration of Re (approx. 5%) and Co compared to the CMSX-4

Table 1. The chemical compositions of CMSX-4 and CMSX-4®Plus SX superalloys

Alloy	Chemical compositions, % wt.									
	Cr	Co	Mo	W	Ta	Al	Ti	Hf	Re	Ni
CMSX-4	6.5	9.0	0.6	6.0	6.5	5.6	1.0	0.1	3.0	bal.
CMSX-4®Plus	3.5	10.0	0.6	5.0	8.0	5.7	0.9	0.1	4.8	bal.

alloy (Table 1). Increased rhenium concentration is expected to strengthen the γ phase and improve creep resistance of the superalloy [18-20]. Classification of the CMSX-4®Plus does not include placement in any of the six generations. However according to the it is most similar to the third – generation of superalloys [18].

The mechanical properties at high temperature of SX superalloys are also influenced by the presence of casting defects, e.g. shrinkage and gas porosity. The porosity is formed as a result of solidification shrinkage or gas entrapment during the crystallization of molten metal. The shrinkage porosity is formed mainly in the interdendritic areas of the casting. The size and relative volume of pores depend on the conditions of the crystallization process. The pore size increases with the distance between primary dendrite arms. Therefore, in the case of nickel-based superalloys it is important to determine the porosity of the casting as well as primary dendrite arms spacing (PDAS) [21-24]. Data on the acceptable level of porosity in single-crystal castings is guarded by global manufacturers of nickel superalloy turbine blades.

Durability of nickel-based SX blades depends strongly on their creep resistance. The characteristics of the high temperature deformation are determined in the creep tests and creep-rupture test. The analysis of obtained creep curves is used to determine the creep speed at specified time. Analysis of creep test results is useful in prediction of turbine blade service time and maintenance intervals of the turbine [3]. Hence, it is recommended to use mathematical models to characterize the creep process.

This paper presents the effect of directional solidification process parameters (withdrawal rate) of the CMSX-4®Plus nickel superalloy on the crystal structure perfection and creep strength. The research described in the article focuses on comparing the obtained high temperature properties of CMSX4®Plus alloy castings and the conventional second generation CMSX-4 alloy. The analysis of microstructure, porosity, crystal perfection and mechanical properties as well as the development of suitable mathematical models for the creep resistance measured during the experiment as a function of time were carried out. The models were built for both investigated materials, i.e., CMSX-4 and CMSX-4®Plus alloys. They were used for verification purposes in the task of developing models of creep and for performing computations for various structural analyzes which consider creep phenomena of investigated alloys.

The equations representing creep in function of time should describe the relation between measurable factors precisely enough and be simple as well as reliable in the cases of considered materials. Therefore, several candidate models were taken into consideration. They were computed as well as arranged in sequence and analyzed in order to select the best model among those taken into account. That model represents an acceptable balance between goodness of fit and parsimony of the model.

One of the results of performed research is the determination of the steady state creep rate . That parameter is used for computations concerning structural analyzes of machine parts, especially high pressure turbine blades and vanes working at elevated temperatures (usually up to 1100 °C). That parameter should be computed based on the obtained experimental data within the range in which the variation of collected data, i.e., the rate of stroke associated with creeping deformation in time is limited and can be approximated using a linear function. The approximation of data should be done heteroscedascity-robust, if possible, to obtain the regression model with unbiased standard errors of ordinary least squares (OLS) coefficients also under heteroscedasticity [25]. In other words, the approximation of collected experimental data should be done in such a way that the OLS estimators are characterized by unbiased standard errors even in the case when the variance of the residual term in a regression model is not constant [26-28]. That case may take place, e.g., when the model is not correctly specified or collected data belong to wide range of observed values. Therefore, application of the heteroscedascity-robust estimation technique may improve that important feature of mathematical model of creep deformation of a sample in function of time. It can also improve, compared to the standard OLS techniques, the determination of the steady state creep rate $\dot{\varepsilon}$.

The aim of the work was to compare two single crystal nickel superalloys differing mainly in the Re content, on the perfection of the crystal structure and mechanical properties – creep resistance.

MATERIALS AND METHODS

Single crystal CMSX-4 and CMSX-4®Plus superalloys rods in as-cast condition were studied. The lost-wax casting method, including

multilayer ceramic mould preparation, was used to produce single crystal castings. The directional solidification process based on Bridgman method was carried out in a vacuum furnace ALD VIM-IC 2 E/DS/SC (ALD Vacuum Technologies GmbH, Hanau, Germany). The withdrawal rate (v_w) of mould applied was 3 and 5 mm/min. The temperature gradients in solidification made with Bridgman method and withdrawal rates of 3 and 5 mm/min were 33 and 22 K/cm, respectively. The single crystal casting processes were carried out in the Department of Materials Science and Research and Development Laboratory for Aerospace Materials at Rzeszow University of Technology.

Microstructure evaluation of superalloys was performed by light microscopy (LM) using Leica DMI 3000M (Leica Microsystems, Wetzlar, Germany) metallographic microscope and Leica Application Suite v3.7 image analysis software. Samples for LM observation were prepared by chemical etching in a solution containing 3g MoO_3, 100 cm^3 HCl, 100 cm^3 HNO_3 and 100 cm^3 H_2O. The mean primary dendrite arm spacing (PDAS) was determined for the cross section of SX rods. The porosity was measured on non-etched metallographic samples by LM at the magnification of 50x. For each casting 10, 2.8 mm^2 areas (images) were analyzed. The volume fraction (V_v), and the size distribution (area of pore plane section A_A) of pores was determined using planimetric method.

Determination of crystal orientation was conducted using OD-EFG-1 X-ray diffractometer (Freiberg Instruments, Freiberg, Germany). Crystal orientation analysis of CMSX-4 and CMSX-4®Plus was determined using Ω-scan method [7]. The α_z angle – deviation of the [001] crystallographic direction from the withdrawal direction Z, was measured on the cross-section of the SX rods to obtain the 2D maps of its deviation.

Creep tests were carried out to determine the creep resistance of single crystals of the CMSX-4 and CMSX-4®Plus nickel superalloy. AG LFMZ-30 (Walter + Bai, Löhningen, Switzerland) machine was used. The tests were carried out according to the ASTM E-139-11 standard, using round samples as specified in the ASTM E8 standard (Fig. 2).

The samples were heated to the temperature of 982 °C and held at that temperature for 1 hour. After annealing, the specimens were loaded with a constant axial force causing the initial tensile stress σ = 151.8 MPa. The temperature measurement during the test was determined with the S-type thermocouple – PtRh10-Pt. The test was the basis for determining time to destruction.

RESULTS AND DISCUSSION

Microstructure and creep resistance of superalloys

The microstructure analysis of as-cast single crystal rods showed that directional crystallization process produces dendritic structure with fully developed primary and secondary dendrite arms both in CMSX-4 and CMSX-4®Plus alloys (Fig. 3). The withdrawal rate of ceramic mould during casting process (3 and 5 mm/min) was found to determine the shape of the dendrites and PDAS. On the contrary, for the CMSX-4 superalloy PDAS decreased from 391 to 355 μm (Fig. 3a, c) with the increase of withdrawal rate from 3 to 5 mm/min (Tab. 2). Similar trend was described in [20], where it was found that PDAS decreased in the range of the withdrawal rate between 1 and 5 mm/min and then increased for castings produced at

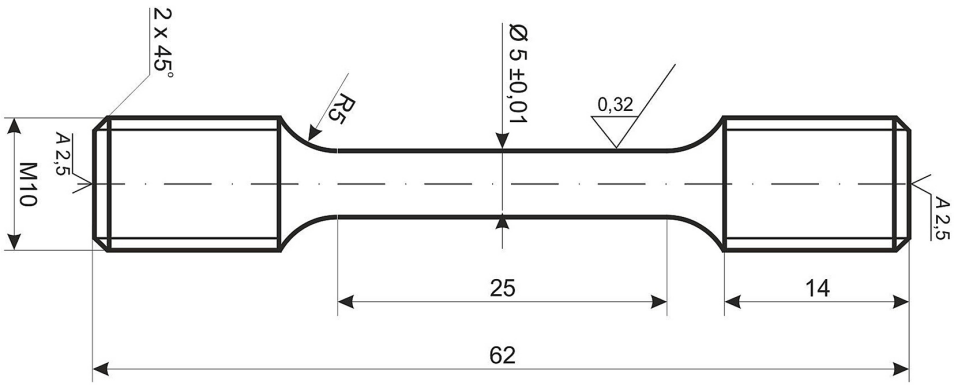

Fig. 2. Dimensions of the samples used for creep tests

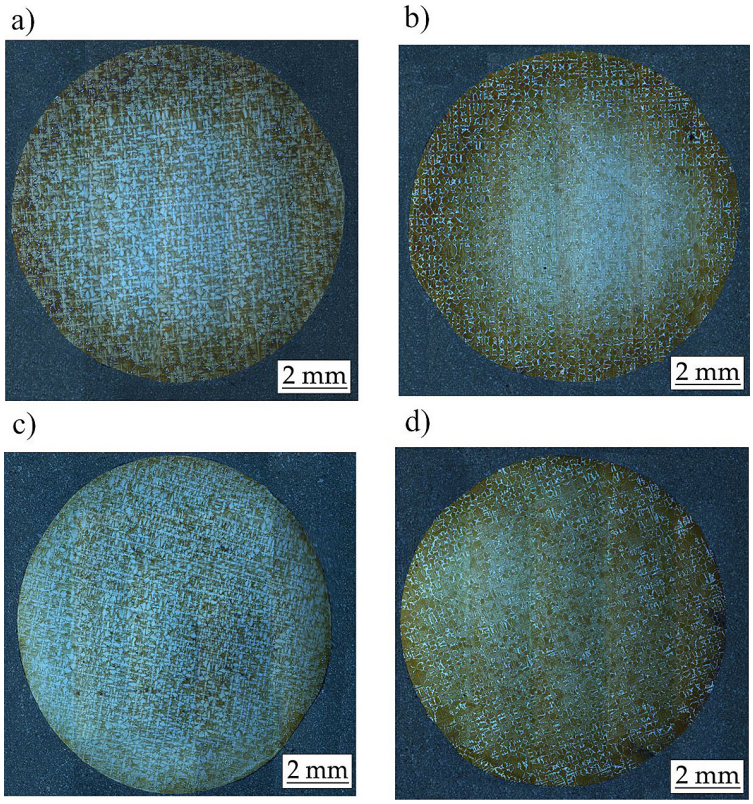

Fig. 3. Dendritic microstructure (LM) of single crystal CMSX-4 (a, c) and CMSX-4®*Plus* (b, d) superalloys rods produced at different withdrawal rate: a, b) 3 mm/min, c, d) 5 mm/min

the withdrawal rate between 5 and 7 mm/min. For CMSX-4®Plus nickel superalloy PDAS increased from 318 to 360 µm (Fig. 3b, d) for the withdrawal rates 3 and 5 mm/min, respectively. It can be therefore assumed that in the case of CMSX-4®Plus superalloy, the trend to increase PDAS should occur already at the withdrawal rate range of 3-5 mm/min which is lower than in the case of conventional single crystal CMSX-4 superalloy (5÷7 mm/min) [21]. However it is little information published on the properties of the CMSX-4®Plus superalloy and especially its PDAS. The presented research tries to fill at least to some extent that gap. It can reasonably be expected that the increased concentration of heavy elements such as rhenium and cobalt in the CMSX-4®Plus superalloy causes that the PDAS will increase at a lower single crystal withdrawal rate.

Table 2. The distance between primary dendrite arm spacing of the CMSX-4 and CMSX-4®*Plus* nickel superalloys

Superalloy	Withdrawal rate v_w, mm/min	Primary dendrite arm spacing PDAS, µm (σ)
CMSX-4	3	391 (19)
	5	318 (15)
CMSX-4®Plus	3	355 (23)
	5	360 (18)

The crystal orientation measurements of single crystals CMSX-4 and CMSX-4®Plus nickel-based superalloys castings indicate the influence of chemical composition and the withdrawal rate on the value of the α_z angle (Fig. 4). For the CMSX-4 superalloy rods produced at withdrawal rate of 3 mm/min the value of the angle α_z falls within the range from 6 to 7.4° (Fig. 4a). Similar values of α_z were obtained for that superalloy cast at withdrawal rate of 5 mm/min (Fig. 4c). In case of CMSX-4®Plus nickel superalloy and withdrawal rate 3 mm/min, the value of the angle α_z was in the range of 4.6 to 6.4° (Fig. 4b). Hence, the deviation of the α_z angle on the cross-section is slightly higher for the new CMSX-4®Plus alloy. Application of withdrawal rate 5 mm/min for CMSX-4®Plus resulted in decrease of α_z value to 2.2–5° (Fig. 4d). Although the mean value of α_z was reduced by c.a. 2°, the deviation of its value increased to 2.8°. It can therefore be assumed that for CMSX-4®Plus superalloy, the increase of withdrawal rate leads to the increase in the deviation of the α_z angle. Similar values of the α_z angle in CMSX-4 and CMSX-4®Plus superalloys are also reported in papers [7, 10, 20, 24].

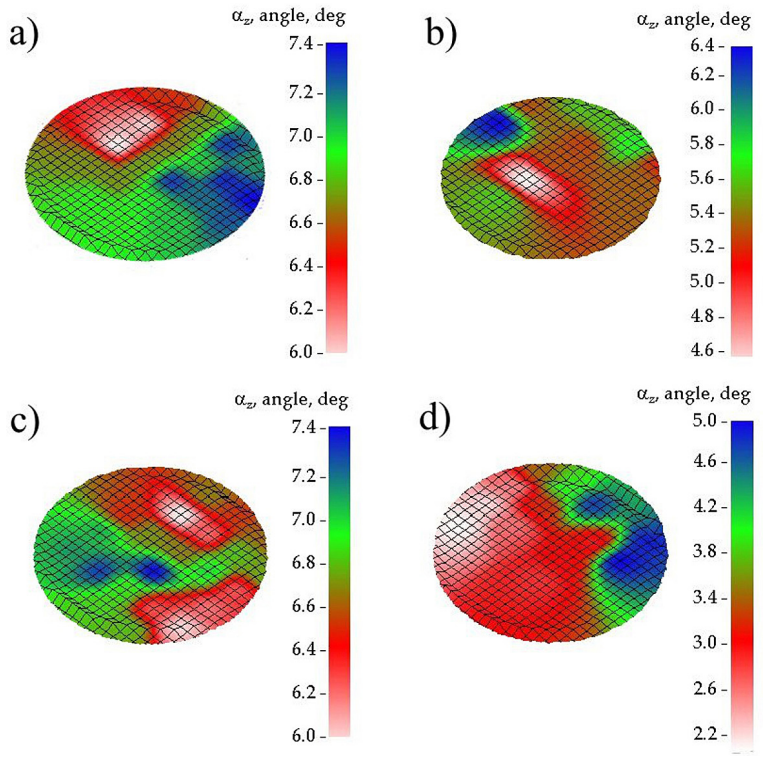

Fig. 4. Value of the α_z angle on the cross-section of the CMSX-4 (a, c) and CMSX-4®Plus (b, d) superalloys produced at different withdrawal rate: a, b) 3 mm/min, c, d) 5 mm/min

Table 3. The distance between PDAS of the CMSX-4 and CMSX-4®Plus nickel superalloys

Alloy	Withdrawal rate v_w, mm/min	Mean volume fraction of pores *Vv*, %	Standard deviation σ_{Vv}, %
CMSX-4	3	0.202	0.044
	5	0.185	0.036
CMSX-4®Plus	3	0.070	0.024
	5	0.069	0.021

Based on the crystal orientation measurements of the CMSX-4 and CMSX-4®Plus nickel-based superalloys, it can be concluded that all castings meet the typical industrial criterion of their usability – the α_z angle value < 10÷15°.

The mean volume fraction of pores *Vv* of the both SX has been determined. Results showed a higher *Vv* content of the CMSX-4 superalloy (Table 3).

In the case of both CMSX-4 and CMSX-4®Plus castings the application of different withdrawal rates, i.e., 3 and 5 mm/min did not led to changes of the *Vv* value. Analysis of the SX castings porosity showed significant differences in the number of pores and their size in CMSX-4 compared with CMSX-4®Plus. In the case of CMSX-4 superalloy castings, regardless of the withdrawal rate, the majority of pores were in the range of 10–50 μm^2 (Fig. 5). At the withdrawal rate 5 mm/min single cases of pores over 200 μm^2 were observed. Although samples produced at the withdrawal rate of 3 mm/min showed lower porosity, i.e., smaller number of pores, the formation of large area pores > 200 μm^2 was also observed.

CMSX-4®Plus castings showed the bigger porosity at the withdrawal rate of 3 mm/min. The pores size was in the range of 0–50 μm^2. A small number of pores with the area bigger than 100 μm^2 was observed in rod cast both at the withdrawal rates of 3 and 5 mm/min (Fig. 6). Moreover, it was found that withdrawal rate in the range 3–5 mm/min has a negligible influence on the volume fraction of pores. Similar observations for CMSX-4 superalloy were established in the paper [21].

It can be concluded that CMSX-4 is characterized by higher volume fraction of pores compared to CMSX-4®Plus. Additionally CMSX-4 has exhibited higher mean area of pore plane section A_A.

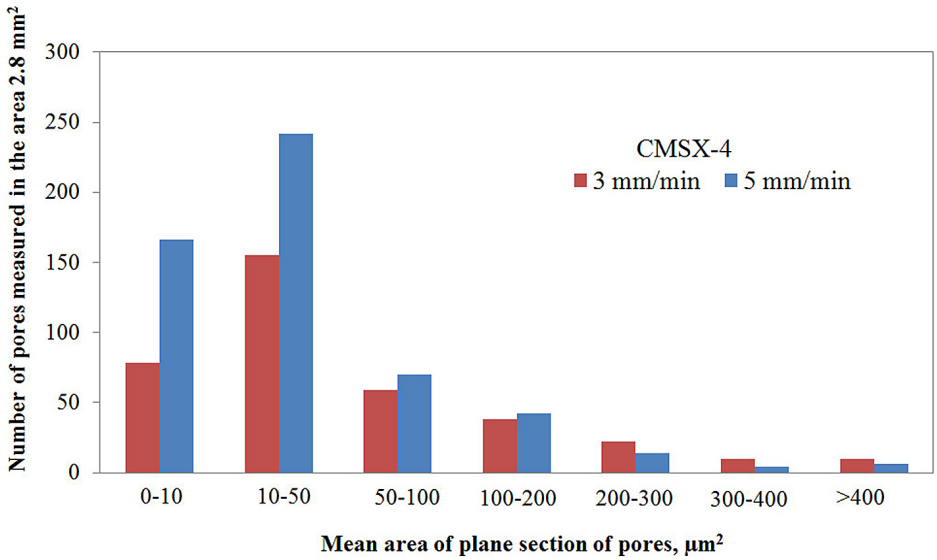

Fig. 5. The number of pores and their average area measured in the cross-section of the CMSX-4 casting

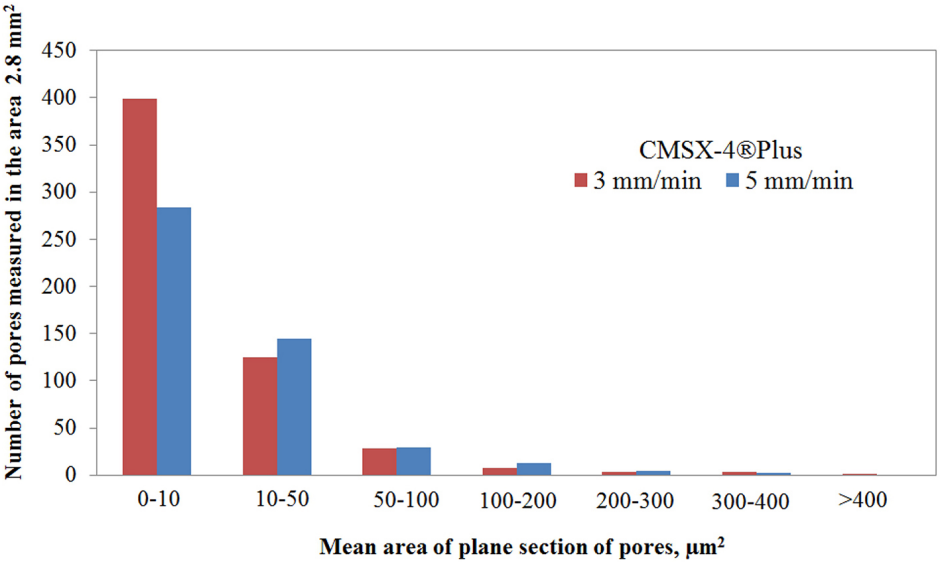

Fig. 6. The number of pores and their average area measured in the cross-section of the CMSX-4®Plus casting

The obtained creep test results showed significant differences in the mechanical properties of CMSX-4 and CMSX-4®Plus nickel superalloys. CMSX-4 superalloy, castings produced at the withdrawal rate of 3 mm/min showed slightly better creep resistance compared to castings made at the withdrawal rate of 5 mm/min, i.e., 108 and 99 h, respectively. The creep test results obtained for CMSX-4®Plus, showed that the time to failure was similar for single crystals produced at withdrawal rates of 3 and 5 mm/min. The time to failure was between 206 and 212 h (Table 4), which also was much higher value compared to the conventional CMSX-4. Simultaneously, more than twice creep resistance for CMSX-4®Plus superalloy was obtained than developed in papers [18, 19].

The creep tests and porosity measurement results indicate the influence of the number and size of pores on the creep strength and time to failure.

Table 4. The time to failure CMSX-4 and CMSX-4®Plus nickel superalloys. Creep test: σ = 151.8 MPa, T = 982 °C

Superalloy	Withdrawal rate v_w, mm/min	Time to failure, h
CMSX4	3	108
	5	99
CMSX-4®Plus	3	206
	5	212

CMSX-4 superalloy produced at the withdrawal rate of 3 mm/min, exhibited 9 h longer time to failure compared to the one made at 5 mm/min. That fact can be associated with a higher mean area of pore plane section A_A. in the case of the CMSX-4®Plus superalloy. Similar observation was made for CMSX-4®Plus superalloy, where lower porosity in single crystals cast at withdrawal rate of 5 mm/min showed time to failure extended by 6 h compared to the castings produced at 3 mm/min.

The statistical models of experimental data

Mathematical models used for the approximation of collected experimental data were polynomial models denoted ST*i*, where *i* represents the degree of polynomial. The lowest degree of polynomial used for modeling creep phenomenon in the whole range of the time of experiment was 3 (model ST3). The intermediate degree was 4 (model ST4) and the highest degree was 5 (model ST5). The general structure of polynomial model in the most developed form taken into account, i.e. model ST5, is represented by the following formula:

$$S(t) = a_0 + a_1 \cdot t + a_2 \cdot t^2 + \\ + a_3 \cdot t^3 + a_4 \cdot t^4 + a_5 \cdot t^5 \quad (1)$$

where: $S(t)$ – stroke in mm as a function of time in hours;
t – time of observation in hours;
a_0, a_1, a_2,..., a_5 – estimated coefficients of the regression model (Eq. 1).

The model (Eq. 1) is nonlinear in general. However, taking into consideration the consecutive monomials t^0, t^1, t^2,...,t^5 as the appropriate base interpolation functions in the regression model and the independent variables, the model becomes linear and the estimators a_0, a_1, a_2,..., a_5 of the regression model (Eq. 1) can be determined using linear approach and the Least Squares (LS) criterion [27-29]. The results of computations for each of the investigated four material cases (MCs) of tested material samples are presented in Tables 5-6. They are denoted: 3CMSX4 for 3 mm/min CMSX-4 sample, 3CMSX4+ for 3 mm/min CMSX-4®Plus sample, 5CMSX4 for 5 mm/min CMSX-4 sample and 5CMSX4+ for 5 mm/min CMSX-4®Plus sample.

In all considered regression models the estimated polynomial coefficients were statistically significant at the 1% level as far as the *p*-value representing the probability value for the statistical test is concerned. Analysis of computed estimators leads to the general conclusion that the successive coefficients a_i with indices changing from 0 to 5 decrease their values. The larger the index number, the smaller the value of the coefficient, compared to the largest value of the calculated coefficients, i.e., the constant estimator. However, one should not eliminate coefficients with small values from the model as they are multipliers of monomials with increasing exponents. Such monomials increase for all values *t* bigger than 1. Due to this fact, removing the regressors with small estimators from the model leads to significant errors in the estimation of experimental

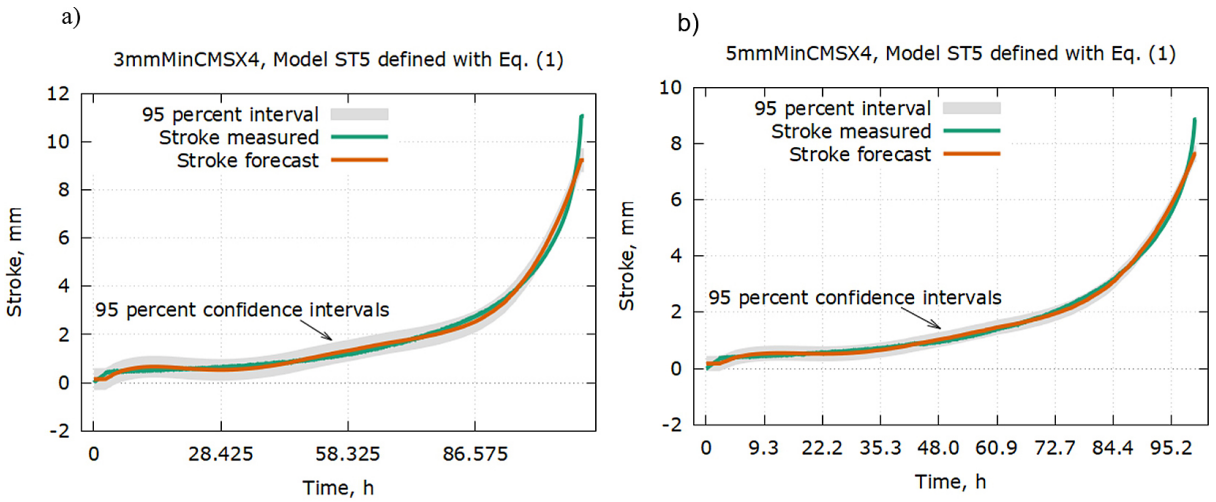

Fig. 7. Measured (Stroke measured) and estimated (Stroke forecast) values of stroke in function of time S(t) (Eq. 1 and Table 4) with the 95% confidence intervals computed at the discrete values of time associated with the measurement serial numbers for the models: a) 3 mm CMSX-4 and b) 5 mm CMSX4

data using the regression model. Therefore, the above mentioned coefficients with small values were not eliminated from the mathematical model defined with Eq. (1).

Basic information about observations and some important heteroscedasticity-robust standard errors of developed regression models referenced in Table 5 are presented in Table 6. The standard errors of regression are more than 500 times smaller in the models MC 1 and 2 and more than 200 times smaller in the models MC 3 and 4 compared to the corresponding sums of squared residuals. Moreover, the fact that the adjusted R^2 parameter is in all cases equal to about 0.99 and that the Fisher-Snedecor test, called *F*-statistic leads to the corresponding *p*-values (*F*) below 0.05 allows to reject the null hypothesis that the developed regression ST5 models *S(t)* (Eq. 1) are insignificant at least at the 5% level. That value of the significance level $\alpha = 0.05$ is the probability of rejecting the null hypothesis when it is true. That value is usually applied in industrial experiments.

Both measured and estimated values of stroke in function of time with the 95% confidence intervals computed for the models 3mmCMSx4 and 5mmCMSX4 (Table 5) at the discrete values of time associated with the measurement serial numbers are shown in Figs. 7a and 7b, respectively.

The computed adjusted R^2 parameter (Table 6) can be interpreted as one of indicators for model selection. It is an acceptable balance between goodness of fit and thriftiness of the model. By definition the adjusted R^2 for linear models computed according to the LS criterion is defined by the following formula [27-29]:

$$\bar{R}^2 = 1 - \frac{SSR/(n-k)}{TSS/(n-1)} \tag{2}$$

where: n – the number of observations in the sample;
k – the number of estimated parameters;
SSR – the sum of squared residuals;
TSS – the total sum of squares for the dependent variable. That coefficient considers the number of regressors in the sense that it penalizes the models with increasing number of parameters. In that sense it represents the goodness of model selection better than the unadjusted R^2, defined by the following formula:

$$\bar{R}^2 = 1 - \frac{SSR}{TSS} \tag{3}$$

The standard error of regression given in Table 6 can be calculated using the following formula:

$$\hat{\sigma} = \sqrt{\frac{SSR}{n-k}} \tag{4}$$

The *F*-statistic is applied to find out, using statistical approach based on the *F*-Snedecor test, whether the regressors being independent

Table 5. The estimated coefficients of regression models with polynomial structure ST5 defined with Eq. (1) representing measured stroke S(t) [mm] as a function of time t [h], based on collected data form creep experiments for all investigated material cases MC with different materials

Case (MC), material and computed estimators for polynomial models ST5							
MC	Material	a_0	a_1	a_2	a_3	a_4	a_5
1	3mmCMSX4	0.144247	0.110388	−8.02453e-3	2.30366e-4	−2.72088e-6	1.15855e-8
2	3mmCMSX4+	0.096174	0.049026	−1.88698e-3	2.91450e-5	−1.83938e-7	4.22140e-10
3	5mmCMSX4	0.173670	0.0793415	−5.98661e-3	1.89303e-4	−2.46450e-6	1.17001e-8
4	5mmCMSX4+	0.370613	0.053533	−1.88503e-3	2.76650e-5	−1.67750e-7	3.71885e-10

Table 6. Basic information about observations and some important heteroscedasticity-robust standard errors of developed regression models ST5 defined with Eq. (1) and referenced in Table 1 representing measured stroke S(t) [mm] as a function of time t [h]

Case (MC), material and heteroscedasticity-robust standard errors for polynomial models ST5							
MC	Material	Number of observations	Sum of squared residuals	Standard error of regression	Adjusted R^2	*F*-statistic	*p*-value(*F*)
1	3 mm CMSX4	1926	102.3661	0.2309	0.986783	F(5, 1920) = 22175.9	0.0
2	3 mm CMSX4+	3327	90.72905	0.165287	0.995129	F(5, 3321) = 1980.348	0.0
3	5 mm CMSX4	1685	31.74419	0.137501	0.99358	F(5, 1679) = 42444.34	0.0
4	5 mm CMSX4+	3542	245.6947	0.263561	0.987967	F(5, 3537) = 50522.95	0.0

variables in the model have statistically significant effect on the average value of the dependent variable, called also described variable. The $H0$ hypothesis, a proposition, states that the described variable does not depend on any of the independent variables, i.e., the corresponding coefficients a_1, a_2,..., a_m are all equal zero. The alternative hypothesis $H1$ is that the coefficients are different from zero. The p-value of the F-statistic can be compared with the assumed significance level α.

In order to check the correctness of model selection in the sense of choosing the model ST5 from between considered models ST3, ST4 and ST5 a more general criterion than the above described was also used. That was the Akaike information criterion (AIC), usually applied in practice as the first model selection criterion when one is attempting to perform a prediction. It helps to assess the goodness of fit of a regression model, given a particular data set, while taking into consideration how extended the model is, i.e. how many independent variables it contains [30-33].

The AIC focuses on a logarithm of a model's maximum likelihood estimation. That logarithm is interpreted as a measure of fit. The likelihood is some measure of a quality of mapping observed data by a developed model. That information is included in the AIC formula with a negative sign. At the same time the AIC adds a penalty term for the complexity of the model associated with the number of independent variables. That information is in the AIC formula with a positive sign:

$$AIC = -2\log L(\hat{\theta}) + 2k \tag{5}$$

where: θ – the vector of model parameters;

$L(\hat{\theta})$ – the likelihood of considered model based on collected data and evaluated at the maximum likelihood estimate $\hat{\theta}$ of the vector θ;

k – the number of estimated parameters in the developed model. Considering the goodness of fit first and simplicity of the model second the AIC helps with finding some solution, i.e., selecting a model from a given set of models representing relations following the data. Computed values of the Akaike information criterion for considered models ST3, ST4 and ST5 are shown in Table 7.

Table 7. The Akaike information criterion (Eq. 5) computed for various considered regression models ST3, ST4 and ST5 and for experimental cases associated with creep phenomenon of different samples described in Tabs. 1 and 2

Case (MC), material and AIC for polynomial models ST3, ST4 and ST5					
MC	Material	Number of observations	AIC for model ST3	AIC for model ST4	AIC for model ST5
1	3 mm CMSX4	1926	2348.3	1165.8	−174.4
2	3 mm CMSX4+	3327	3451.5	453.6	−2530.0
3	5 mm CMSX4	1685	592.2	−602.7	−1898.7
4	5 mm CMSX4+	3542	3569.0	610.4	−2377.4

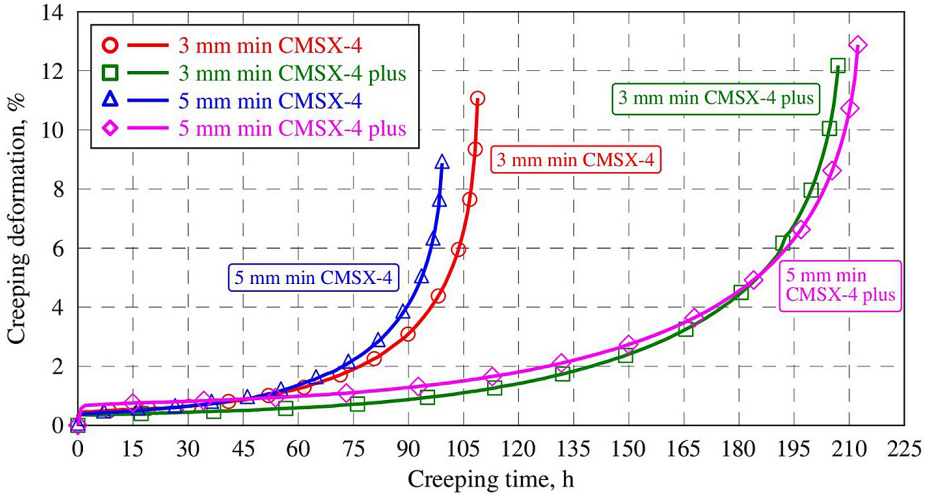

Fig. 8. Measured values of stroke/creeping deformation in function of time S(t) for the samples 3 mm min CMSX-4, 3 mm min CMSX-4 plus, 5 mm min CMSX-4 and 5 mm min CMSX-4 plus

From the data given in Table 7 it follows that if the goodness of fit is a primary concern with consideration to the simplicity of the regression model the model ST5 is the best from all computed models ST3, ST4 and ST5 as its AIC is the lowest in each investigated experimental case of creep. In other words, the model ST5 with the maximum likelihood is the one that "fits" the data the best with not too big number of independent variables, i.e., represents an acceptable balance between the risk of underfitting and the risk of overfitting.

In order to determine the steady state creep rate from experimental data the vector of data was cut at both ends to limit the analysis to the steady state range in which the creeping deformation as a function of time can be approximated with a linear regression model. Therefore, as far as the time of experiment is concerned, in the cases "3 mm CMSX4" and "5 mm CMSX4" the range of analyzed data was limited to < 3, 45 > hours. In the cases "3 mm CMSX4 plus" and "5 mm CMSX4 plus" the range of analyzed data was limited to < 3, 90 > hours (Fig. 8). The limitation of the time range when determining the steady state creep rate was related to the fact that in further calculations the experimental data should represent a linear function as much as possible.

The determination of steady state creep rate $\dot{\varepsilon}$

The steady state creep rate $\dot{\varepsilon}$ was determined as the slope in the linear regression model. The estimators of the developed regression models ST1 defined with Eq. (1), i.e., intercept a_0 and the steady state creep rate $\dot{\varepsilon}$, with some important statistical characteristics – heteroscedasticity-robust standard errors and model goodness of fit indicators as well as related 95% confidence intervals (95%CI) for computed estimators – are presented in Tabs. 8 and 9.

In all considered linear regression models ST1 the estimated polynomial coefficients (Tables 8 and 9) are statistically significant at the 1% level as far as the *p*-value representing the probability value for the statistical test is concerned (Table 9). The standard errors of regression are in average 10 times less than in the case of ST5 regression models (Tables 6 and 7). Moreover, the adjusted R^2 parameter is in all cases not less than 0.96 which means very well goodness of fit. The Fisher-Snedecor tests, *F*-statistic, with the *p*-values (*F*) less than 0.01 allow to reject the null hypothesis that the developed regression ST1 models *S(t)* (Eq. 1) are insignificant at least at the 1% level. That value of the significance level $\alpha = 0.01$ is the probability of rejecting the null hypothesis when it is true [34-36].

Table 8. Basic information about number of observations and coefficients of linear regression model, intercept and steady state creep rate $\dot{\varepsilon}$ with important heteroscedasticity-robust standard errors and model goodness of fit indicators of developed linear regression models ST1 defined with Eq. (1) representing measured stroke S(t) [mm] as a function of time t [h]

Material, heteroscedasticity-robust standard errors and creep rate for polynomial models ST1							
Material	No of observ.	Intercept a_0	Creep rate $\dot{\varepsilon}$	Standard error of regression	Adjusted R^2	*F*-statistic	*p*-value(*F*)
3 mm CMSX4	682	0.408939	8.82649e-3	0.022387	0.958675	F(1, 680) = 12596.83	0.0
3 mm CMSX4+	1350	0.282165	5.67663e-3	0.028465	0.961075	F(1, 1348) = 20956.31	0.0
5 mm CMSX4	657	0.321862	11.6487e-3	0.024058	0.972331	F(1, 655) = 15288.64	0.0
5 mm CMSX4+	1383	0.637349	6.28199e-3	0.028295	0.970265	F(1, 1381) = 30305.63	0.0

Table 9. Computed values of estimators for the intercept a_0 and creep rate $\dot{\varepsilon}$ with their related p-values as well as 95% confidence intervals (95%CI) of developed linear regression models ST1 defined with Eq. (1) representing measured stroke S(t) [mm] as a function of time t [h]

Intercept a_0 and creep rate $\dot{\varepsilon}$ with p-values and 95% confidence intervals for polynomial models ST1						
Material	Intercept a_0	*p*-value(a_0)	95%CI(a_0)	Creep rate $\dot{\varepsilon}$	*p*-value($\dot{\varepsilon}$)	95%CI($\dot{\varepsilon}$)
3 mm CMSX4	0.408939	0.0	(0.405520, 0.412357)	8.82649e-3	0.0	(0.00867208, 0.00898090)
3 mm CMSX4+	0.282165	0.0	(0.278759, 0.285571)	5.67663e-3	0.0	(0.00559971, 0.00575356)
5 mm CMSX4	0.321862	0.0	(0.317553, 0.326171)	11.6487e-3	0.0	(0.0114637, 0.0118337)
5 mm CMSX4+	0.637349	0.0	(0.634329, 0.640369)	6.28199e-3	0.0	(0.00621120, 0.00635278)

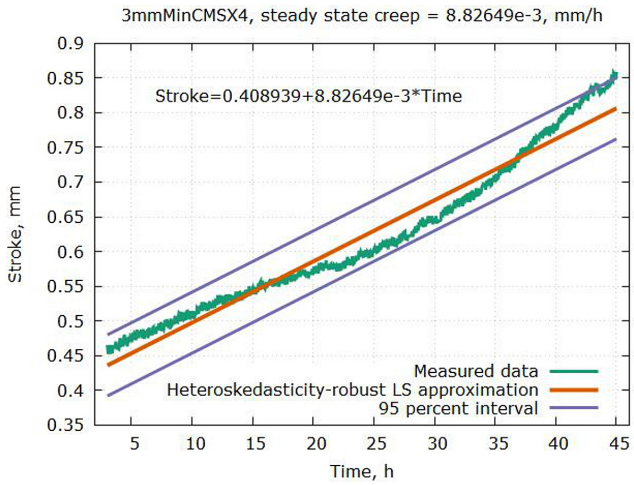

Fig. 9. The developed linear model ST1 i.e., stroke (creeping deformation) in function of time S(t) for the sample 3 mm min CMSX-4 which allowed to determine the steady state creep rate $\dot{\varepsilon}$ in that case with 95% confidence intervals for the dependent variable

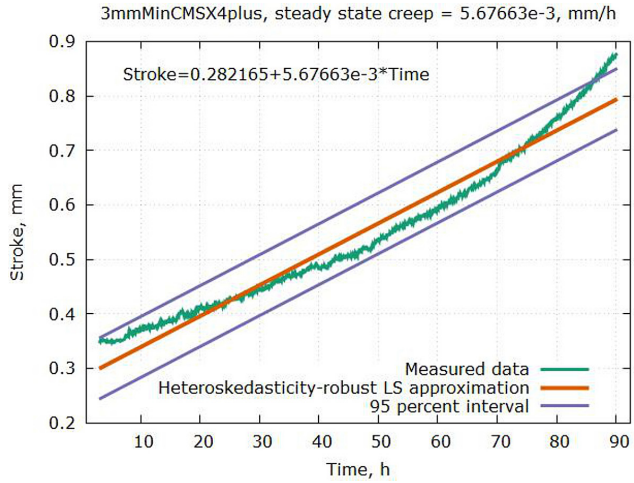

Fig. 10. The developed linear model ST1 i.e., stroke (creeping deformation) in function of time S(t) for the sample 3 mm min CMSX-4 plus which allowed to determine the steady state creep rate $\dot{\varepsilon}$ in that case with 95% confidence intervals for the dependent variable

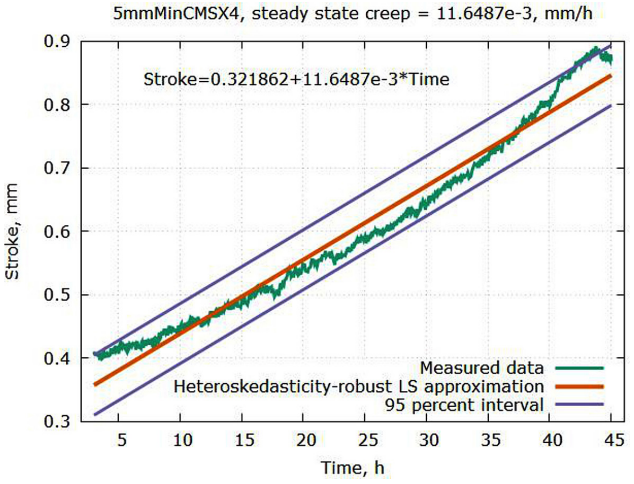

Fig. 11. The developed linear model ST1 i.e., stroke (creeping deformation) in function of time S(t) for the sample 5 mm min CMSX-4 which allowed to determine the steady state creep rate $\dot{\varepsilon}$ in that case with 95% confidence intervals for the dependent variable

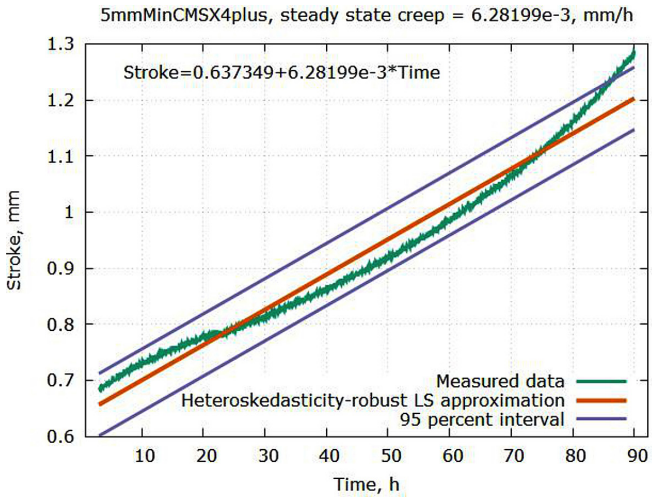

Fig. 12. The developed linear model ST1 i.e., stroke (creeping deformation) in function of time S(t) for the sample 5 mm min CMSX-4 plus which allowed to determine the steady state creep rate $\dot{\varepsilon}$ in that case with 95% confidence intervals for the dependent variable

The developed linear models ST1 which allowed to determine the steady state creep rate for all investigated samples with different materials are presented in graphs with 95% confidence intervals for the dependent variable, i.e., stroke. They are shown in Figs. 9-12.

CONCLUSIONS

The use of the materials presented in the manuscript are most often used for production of high pressure turbine blades in aircraft engines. One of the characteristics of the CMSX-4®Plus superalloy is the increased concentration of Re. Expected use of these material such as manufacture of turbine blades in aircraft engines should have the following characteristics: withdrawal rate at 3 mm/min, low pore content – especially large ones and steady state creep rate as small as possible [1, 3].

The microstructure and crystal structure perfection of the CMSX-4 and CMSX-4®Plus superalloy single crystal (SX) castings produced at the withdrawal rate of 3 and 5 mm/min was evaluated. Based on obtained results the following conclusions can be formulated:

1. Increasing the withdrawal rate of casting from 3 to 5 mm/min leads to a decrease in primary dendrite arm spacing (PDAS) in the CMSX-4 superalloy, while an increase in the case of the new CMSX-4®Plus.
2. The CMSX-4 and CMSX-4®Plus castings have a similar crystal orientation with the deviation angle $\alpha_z < 10°$. The withdrawal rate has no significant effect on the angle α_z.
3. Formation of pores with an average area of plane section bigger than 10 μm^2 was observed in the conventional CMSX-4 superalloy, while their size was considerably smaller in the new CMSX-4®Plus superalloy and ranged from 0 to 10 μm^2.
4. The CMSX-4®Plus superalloy castings produced at the withdrawal rates of 3 and 5 mm/min showed approximately two times longer time to failure during the creep test compared to the CMSX-4 superalloy castings manufactured at the same process parameters.
5. The least steady state creep rate $\dot{\varepsilon}$ was observed for the sample produced from CMSX-4®Plus sample cast superalloy at the withdrawal rate of 3 mm/min while the biggest, almost two times bigger, for the sample produced from CMSX-4 superalloy at the withdrawal rate of 5 mm/min. The above partial conclusions allow to draw the general conclusion that mechanical properties at high temperature of the CMSX-4®Plus are better compared to CMSX-4 superalloy. However, turbine blades made of CMSX-4®Plus must be manufactured at relatively small withdrawal rates, approximately 1–3 mm/min.

Acknowledgements

This work was supported by the National Science Centre Poland (NCN) under Grant No. Preludium-UMO-2016/21/N/ST8/00240.

REFERENCES

1. Reed R.C. The Superalloys, fundamentals and applications. Cambridge University Press, 2006.
2. Reed R.C., Matan N., Cox D.C., Rist M.A., Rae C.M.F. Creep of CMSX-4 superalloy single crystals: effects of rafting at high temperature. Acta Materialia 1999; 47(12): 3367-3381.
3. Pollock T.M., Tin S. Nickel-based superalloys for advanced turbine engines: chemistry, microstructure and properties. Journal of Propulsion and Power 2006; 22(2): 361-374.
4. Miller J.D., Pollock T.M. The effect of processing conditions on heat transfer during directional solidification via the Bridgman and liquid metal cooling processes. Metallurgical and Materials Transactions A 2014; 45: 411-425.
5. Li Y., Liu L., Sun D., Yue Q., Huang T., Gan B., Zhang J., Fu H. Quantitative analysis of withdrawal rate on stray grain formation in the platforms of a Ni-based single crystal dummy blade. Journal of Alloys and Compounds 2019; 773: 432-442.
6. Durand-Charre M. The microstructure of superalloys. Gordon and Breach Science Publishers, 2003.
7. Gancarczyk K., Albrecht R., Berger H., Szeliga D., Gradzik A., Sieniawski J. Determination of crystal orientation by Ω-scan method in nickel-based single crystal turbine blades. Metallurgical and Materials Transactions A 2017; 48: 5200-5205.
8. Bogdanowicz W., Albrecht R., Sieniawski J., Kubiak K., Onyszko A. Correlation between sem and x-ray diffraction imaging of defect structure in single-crystal Ni-based superalloy. Solid State Phenomena 2012; 186: 135-138.
9. Zhang H., Xu Q., Liu B. Numerical simulation and optimization of directional solidification process of single crystal superalloy casting. Materials 2014; 7(3): 1625-1639.
10. Szeliga D., Gancarczyk K., Ziaja W. The control of solidification of Ni-based superalloy single-crystal blade by mold design modification using inner radiation baffle. Advanced Engineering Materials 2018; 20(7): n/a.
11. Li J., Wang Z., Wang Y., Wang J. Phase-field study of competitive dendritic growth of converging grains during directional solidification. Acta Materialia 2012; 60(4): 1478-1493.
12. Das N. Advances in nickel-based cast superalloys. Transactions of the Indian Institute of Metals 2010; 63: 265-274.
13. Sato A., Harada H., Yeh A.C., Kawagishi K., Kobayashi T., Koizumi Y., Zhang J.X.A. 5th generation SC superalloy with balanced high temperature properties and processability. In: Proc. of the 11th International Symposium on Superalloys, Pittsburgh, USA 2008, 131-138.
14. Blavette D., Caron P., Khan T. An atom probe study of some fine scale microstructural feature in nickel base single crystal super alloys. In: Proc. of the 6th International Symposium on Superalloys, Seven Springs, USA 1988, 305-314.
15. Rezaei M., Kermanpur A., Sadeghi F. Effects of withdrawal rate and starter block size on crystal orientation of a single crystal Ni-based superalloy. Journal of Crystal Growth 2018; 485: 19-27.
16. Ma D., Wang F., Wu Q., Bogner S., Bührig-Polaczek A. Innovations in casting techniques for single crystal turbine blades of superalloys. In: Proc. of the 13th International Symposium on Superalloys, Warrendale, USA 2016, 237-246.
17. Yoshitake S., Narayan V., Harada H., Bhadeshia H.K.D.H., Mackay D. Estimation of the γ and γ' lattice parameters in Nickel-base superalloys using neural network analysis. ISIJ International 1998; 38(5): 495-502.
18. Wahl J.B., Harris K.K. Improved 3rd generation single crystal superalloy CMSX-4 Plus (SLS) – a study of evolutionary alloy development. Cannon-Muskegon Corporation, 2018 [19] Wahl J.B., Harris K.K. CMSX-4 Plus single crystal alloy development, characterization and application development. In Proc. of the 13th International Symposium on Superalloys, Warrendale, USA 2016, 25-33.
19. Gancarczyk K., Zubko M., Hanc-Kuczkowska A., Kościelniak B., Albrecht R., Szeliga D., Motyka M., Ziaja W., Sieniawski J. The effect of withdrawal rate on crystal structure perfection, microstructure and creep resistance of single crystal castings made of CMSX-4 Nickel-based superalloy. *Materials* 2019; 12(20): n/a.
20. Jaroszewicz J., Matysiak H., Michalski J., Matuszewski K., Kubiak K., Kurzydłowski K. Characterization of single-crystal dendrite structure and porosity in nickel-based superalloys using x-ray micro-computed tomography. Advanced Materials Research 2011; 278: 66-71.
21. Anton D., Giamei A. Porosity distribution and growth during homogenization in single crystals of a nickel-base superalloy. Materials Science and Engineering 1985; 76: 173-180.
22. Long H., Mao S., Liu Y., Zhang Z., Han X. Microstructural and compositional design of Ni-based single crystalline superalloys – a rewiew. Journal od Alloys and Compounds 2018; 743: 203-220.
23. Krawczyk J., Paszkowski R., Bogdanowicz W., Hanc-Kuczkowska A., Sieniawski J., Terlecki B. Defect creation in the root of single-crystalline turbine blades made of Ni-based superalloy. Materials 2019; 12(6): n/a.
24. Johnston J, DiNardo J. Econometric methods (4th ed.). McGraw Hill Higher Education, 1997.
25. Engle R. F. Autoregressive conditional heteroscedasticity with estimates of the variance of united

kingdom inflation. Econometrica,1982; 50(4): 987-1007.

26. Draper N.R., Smith H. Applied regression analysis (3rd ed.). John Wiley & Sons, 1998.
27. Fox J. Applied regression analysis, linear models and related methods. Sage Publications, 1997.
28. Sen A., Srivastava M. Regression analysis - theory, methods, and applications. Springer-Verlag, 1990.
29. Akaike H. A new look at the statistical model identification, IEEE Transactions of Automatic Control 1974; 19(6): 716-723.
30. Giraud C. Introduction to high-dimensional statistics. CRC Press, 2015.
31. Konishi S., Kitagawa G. Information criteria and statistical modeling. Springer-Verlag, 2008.
32. Burnham K.P., Anderson D.R. Model selection and multimodel inference: A practical information-theoretic approach. Springer-Verlag, 2002.
33. Dekking F.M. A modern introduction to probability and statistics: understanding why and how. Springer, 2005.
34. Cox D.R., Hinkley D.V. Theoretical statistics. Chapman & Hall, 1974.
35. Montgomery D.C., Runger G.C., Hubele N.F. Engineering statistics. Wiley, 2011.